Modelling instrument background for CCD x-ray spectrometers in space

Journal Item

For guidance on citations see FAQs.

oro.open.ac.uk

Modelling instrument background for CCD X-ray spectrometers in space

David Hall[*a], Andrew Holland[a] and Martin Turner[b]

[a] e2v centre for electronic imaging, School of Engineering and Design,
Brunel University, Uxbridge, Middlesex, UB8 3PH, UK
[b] Space Research Centre, University of Leicester,
University Road, Leicester LE1 7RH, UK

ABSTRACT

The European Space Agency (ESA) X-ray Evolving Universe Spectroscopy (XEUS) mission is designed as a follow-on to the ESA X-ray Multi Mirror (XMM-Newton) mission and may contain charge-coupled device (CCD) based instrumentation. Low instrument background is essential for the mission to maximise sensitivity. Results from XMM-Newton and the Japanese Space Agency Suzaku mission show that both the detector design and the orbit (LEO vs. HEO) have major impacts on the instrument background. This gives implications for the optimal instrument configuration for XEUS and other future missions. Here we use a Monte Carlo simulation technique, utilising the Geant4 toolkit, to model the instrument background for CCDs in-orbit. The model will be initially verified by simulating the background from the XMM-Newton and Suzaku missions and comparing this to real data obtained in-orbit. The simulated data will then be analysed to gain a better understanding of the cause of the background. Suggestions for minimizing the instrument background in future missions based on the results found here are included.

Keywords: Instrument background, XMM, Suzaku, XEUS, EDGE, Geant4, CCD X-ray spectrometer, cosmic-ray

1. INTRODUCTION

Instrument background signal is one of the many sources of background encountered when using CCD X-ray spectrometers in space. Internal background due to the electronics within the detector, such as dark current in the CCD, is usually insignificant when compared to sources of background external to the detector. The two most significant forms of background are those caused by detection of unwanted signal through the aperture of the detector and the instrument background through cosmic-rays interacting with the detector and the surrounding materials. The instrument background is studied here in detail for two missions: the Japanese Space Agency Suzaku mission and the ESA XMM-Newton mission. These missions were chosen due to the differing orbits and the ready availability of background data taken in-orbit.

Below 2 keV the instrument background does not dominate and the spectrum is dominated by undesired signal through the detector aperture. Above 2 keV, however, it is the instrument background which dominates and the level of the instrument background can thus play a major part in the quality of results obtained.

The design of the CCD detectors and surrounding materials can have a considerable effect on the background, as is seen in Section 6. The missions studied here each use two different designs of detector and the resulting effects of the mission orbit and detector design on the instrument background is examined in detail.

The two missions (XMM-Newton and Suzaku) are described in Sections 2-5, noting the information of most importance to this study: the orbit and the detector construction. The orbit determines the particles which will be incident on the material surrounding the detectors, which will in-turn affect the spectrum of particles incident on the detectors themselves. The detector construction will then affect how these particles are "interpreted" in the resulting data.

The simulations were executed using the Geant4 toolkit. Quoting the Geant4 website: "Geant4 is a toolkit for the simulation of the passage of particles through matter. Its areas of application include high energy, nuclear and accelerator physics, as well as studies in medical and space science" (http://geant4.web.cern.ch/geant4). The toolkit allows the implementation of Monte Carlo based simulations of particles through matter using code written in C++. The code is required to specify the detector construction, the incident particle spectrum and the logging of data. The data logged by the Geant4 simulation is then analysed; first by running a selection of purpose-written code and then through further analysis using MATLAB.

2. THE XMM-NEWTON MISSION

XMM-Newton was launched on December 10th 1999 into an operational orbit with a perigee of approximately 7 000 km and an apogee of 120 000 km. At this orbit the mission was predicted to experience "close to interplanetary galactic cosmic ray spectra at solar minimum conditions" [1]. Although the pn-CCD camera and MOS CCD camera operate in slightly different ways, the process of modelling the background is not affected.

2.1 The detectors

The XMM-Newton mission contains two types of CCD based detectors: two MOS CCD cameras (MOS1 and MOS2) and one pn-CCD camera. These will be referred to as the MOS and the pn respectively from this point forward. The construction of the detectors is shown in Table 1. The MOS and front-illuminated CCD (FI-CCD) are similar in the way the instrument background is formed. The pn and back-illuminated CCD (BI-CCD), although operationally different, are similar in nature in terms of instrument background and in the way they differ from the MOS and FI-CCD.

2.2 The surroundings

For the XMM-Newton simulation a simple aluminium spherical shell of inner radius 45 mm and thickness 3 cm was used to represent the material surrounding the CCD detectors. This approximation is explained in Section 4.2.

Table 1. The construction of the XMM-Newton detectors as used in the simulations. The *sensitive detector* is the part of the structure in Geant4 in which data is collected. The electrode structure was initially modelled using a simple 1 micron thick SiO_2 layer. This was later updated to provide a more accurate model of the structure.

Layer	MOS	pn
Electrode structure	~1 µm	-
Si sensitive detector	~30 µm	~300 µm
Si field-free region and substrate	600 µm	-
Cu layer (on PCB)	-	100 µm
Pixel size	40 µm	150 µm

2.3 The in-orbit out of field of view background

For XMM-Newton, the out of field of view background is dominated by the instrument background. The out of field of view area of the CCDs corresponds to the overlapped regions of the seven MOS CCDs forming the focal plane and the corners outside of the circular field of view area for both the MOS and pn. The MOS in-orbit data was acquired with thanks to Andrew Read at the University of Leicester and the in-orbit pn data taken from [2]. The approximated continuum is shown for ease of comparison in Figure 1.

The instrument background for the pn is approximately three times higher than that for the MOS when comparing single pixel events. The general spectral form is that of the continuum shown as the approximation in Figure 1. It is this continuum that the simulation aims to recreate.
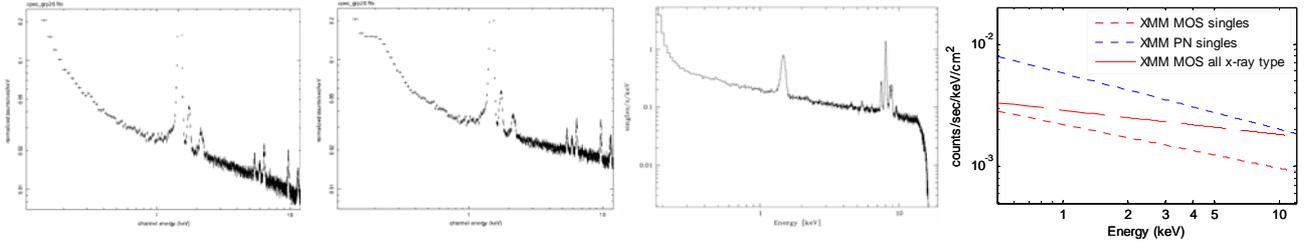
Figure 1. XMM-Newton out of field of view background. *From left to right:* 1. MOS single pixel events. 2. MOS all X-ray grade events. Images used courtesy of Andrew Read, University of Leicester. 3. pn single pixel events, [2]. 4. Comparison of approximated spectra (continua only).

3. THE XMM-NEWTON MODEL

Data was simulated for the two detector types: the MOS and the pn. The first results shown here were taken using the basic model as in Table 1. The initial analysis is based on these results.

3.1 Incident particle spectrum

The orbit of XMM-Newton is at a much higher altitude than Suzaku and so the detectors are subject to a different flux of particles. At this higher orbit the galactic cosmic rays are predominantly ionised nuclei. These ionised nuclei are dominated by protons (approximately 95%). From results for the Suzaku simulation (Section 6.2), where only a few percent of the incident particle flux consist of protons, it is seen that the protons cause a significant proportion of the instrument background. At the orbit of XMM-Newton, where protons dominate the incident particle flux, these protons should therefore be the dominant cause of the instrument background.

A simple incident proton spectrum of the form Energy^{-2} is used. Protons below 80 MeV are absorbed in the 3cm of aluminium. The initial results were taken for incident protons of energy 100 MeV, with further energies included after initial testing.

A rate of 2-2.5 protons cm^{-2} s^{-1} was found for protons passing through the detectors in [1] by counting the tracks through the detectors from in-orbit data. This rate was found to be consistent with a rate of 4.4 cm^{-2} s^{-1} in solar minimum conditions, reduced by a factor of two at solar maximum due to solar modulation. The total rate of incident protons is normalised to this value.

3.2 Data analysis

To produce these results, as shown in Figure 4, the simulation ran as described previously with separate code being used to analyse the results. For the pn, the code sums the energy deposited in each pixel on a second by second basis and all events which are not confined to a single pixel are rejected. For the MOS detector the analysis was more complicated. Charged particles passing through the MOS detector leave long tracks which are subject to charge spreading in the lower regions of the silicon. This leads to the signal being rejected due to spreading across multiple pixels. A simple model was used to avoid the implementation of charge spreading code. If a proton had passed through the pixel during the frame in which the energy was being summed then this pixel would be ignored. All events which involve electrons passing through to the underside of the silicon were rejected as they would have passed through a large thickness of silicon to reach this point and hence would be subject to charge spreading over several pixels. Events were split into grades based on the layout of the signal in the pixels and then split into single pixel events, all X-ray grade events and rejected events.

4. THE SUZAKU MISSION

Following the unsuccessful launch of the JAXA ASTRO-E satellite in 2000, a second mission, ASTRO-EII, was launched on July 10th 2005. After a successful launch the mission was nicknamed Suzaku, meaning "red bird of the south". The mission has not been without its problems, with a vacuum system malfunction effectively shutting down the main instrument: the X-ray Spectrometer (XRS). The CCD detectors were fortunately left unaffected. It is these detectors which are studied here.

4.1 The detectors

The Suzaku mission incorporates four X-ray Imaging Spectrometer (XIS) CCD detectors of two types: three front-illuminated CCDs (XIS0, XIS2, and XIS3) and one back-illuminated CCD (XIS1). These will be simply referred to as the FI-CCD and BI-CCD respectively from this point forward. The construction of these detectors as used in these simulations is shown in Table 2 and is taken from [3].

Table 2. The construction of the Suzaku detectors as used in the simulations here. The *sensitive detector* is the region of the structure in which data is collected.

Layer	FI	BI
SiO_2 electrodes	0.7µm	-
Si sensitive detector	70 µm	45 µm
Si field-free region and back diodes	605 µm	-
Pixel size	24 µm	24 µm

4.2 The surroundings

The surroundings of the detectors are an important factor in the model structure. Murakami *et al.* [3] studied the background of the Suzaku mission and tested their simulation with two structures. Firstly, they created a realistic model of the whole XIS detector. Secondly, as a comparison, they created a simple model consisting of a spherical shell of aluminium with the appropriate density profile. They found that the spectrum of particles reaching the detector in both models was very similar and suitable to enable the use of the spherical model. This simplified model requires less computational time due to the reduced complexity of the particle tracks.

4.3 The in-orbit background (closed filter)

The in-orbit background taken with a closed filter is dominated by the instrument background. The data is shown here in Figure 2, with the in-orbit data and the approximation that has been used for ease of comparison. It is clear from this data that the BI-CCD has a higher level of instrument background than the FI-CCDs. The spectra here are more complex than those in the XMM-Newton detectors but they are also subject to a different incident cosmic-ray spectrum, so this is to be expected. Explanation of the spectral form is left to Section 6.
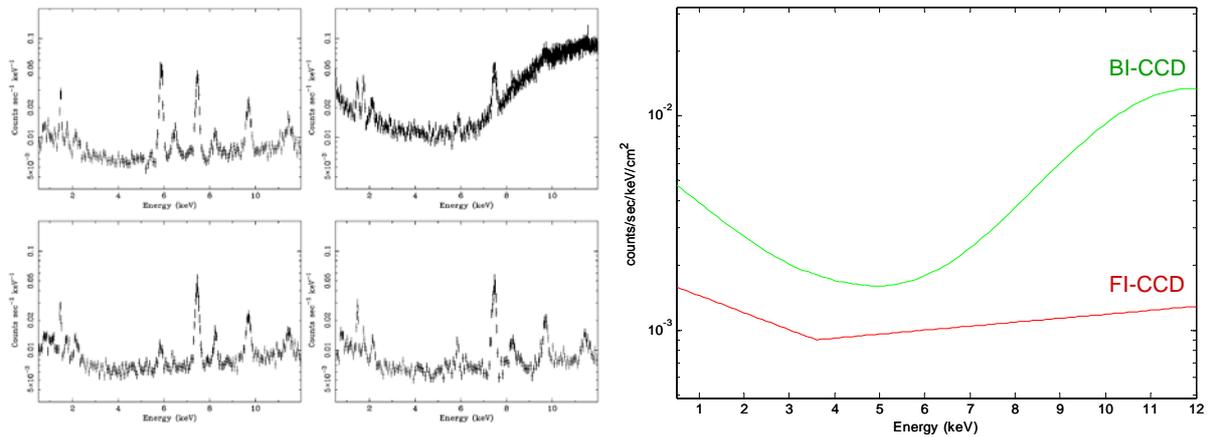

Figure 2. *LEFT*: The in-orbit (closed filter) spectra for Suzaku. The background for the BI-CCD is shown on the top right, with the three FI-CCDs shown in the remaining three quadrants. Image reproduced with thanks to Hiroya Yamaguchi. *RIGHT*: The approximated spectrum of the background for the BI-CCD (upper) and the average for the FI-CCDs (lower) for ease of comparison, with the scale being converted to counts/sec/keV/cm^2.

5. THE SUZAKU MODEL

Data was simulated for the two detector types: the FI-CCD and the BI-CCD. The models used for the detectors have been shown previously in Table 2. The incident particle spectrum is an approximation used to save processing time, and is thus not completely accurate. The flux of each particle type was determined using the integral of the spectrum shown in Figure 3 and normalised to 0.6 protons per cm^2 per second. In order to generate a suitably scaled spectrum when running the simulation it was necessary to take a set total of each particle per second. This value was taken as the integral between two energies of the real spectrum. This was required to save processing time. The spectrum in the simulation was generated using a Monte Carlo method of "accept or reject" by generating two random numbers, the energy and the "flux", and comparing these to the spectral form. As the spectral forms of the incident particle spectra have very steep gradients, a small increase in the energy band considered significantly increases the processing time. The energy bands used were taken as the regions dominating the background.

This provides a good scaling of the different regions of the instrument background, but the flux is out by a factor of 3-4. A similar problem was found in [3] where they believed that the approximations used in the model were causing a shift in their results by a constant factor.

5.1 Data analysis

The code used to analyse the data output from the GEANT4 simulations for each detector type was based on the same underlying code, but with small variations between the two detector types. For the BI-CCD, the energy deposited in each pixel was summed on a second by second basis and non-X-ray grade events were rejected. In this way the single, double, triple and quadruple pixel events were all included. In the case of the FI-CCD, higher energy charged particle tracks were rejected. In the FI-CCD these charged particles would leave a long track in the silicon which would be subject to charge spreading over several pixels in the lower regions of the detector.

5.2 Incident particle spectrum

Suzaku has a low-earth-orbit (LEO) at approximately 570 km above the Earth's surface. At this orbit, the main components of the cosmic-ray spectrum are protons, electrons and photons. Past studies, [3] and [5], describe this spectrum in detail and it is an approximation to this spectrum which is used. The energy bands in Figure 3 show the regions in the spectrum which are used in this simulation.

When a high energy proton passes through the CCD detectors a clearly defined track can be seen. These tracks can be counted from the in-orbit data and the flux of protons incident on the detectors can be calculated. Using results from [3] to calculate a rate of 0.6 protons cm^{-2} s^{-1} in the detector, the incident particle flux can be normalised to provide a more accurate incident particle rate.

Particles incident on the system are generated at a random position on the outer surface of the aluminium shell to be uniformly distributed in area. A second point on the outer surface of the aluminium is then randomly generated and the vector calculated between these two points. This vector is taken as the initial direction of the particle. This gives an isotropic set of incident particles.
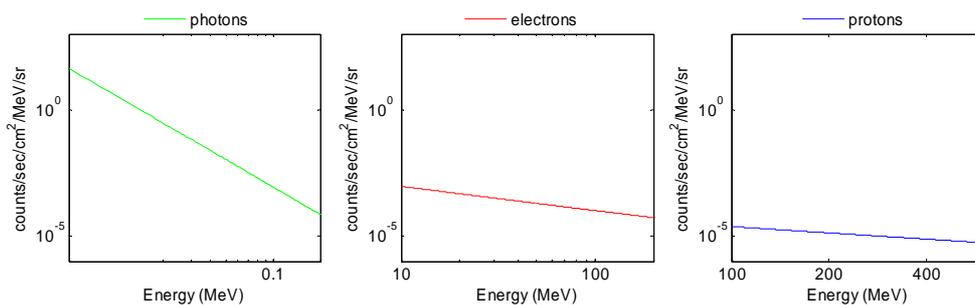

Figure 3. The approximated Suzaku incident cosmic-ray spectrum. The spectra here are different to those found at the XMM-Newton orbit. Much of the electron and photon flux can be attributed to secondaries from the protons found at the orbit of XMM-Newton. The energy regions shown represent the dominating regions of the spectrum. Below these energies the particles do not have sufficient energy to penetrate the shielding.

6. RESULTS AND DISCUSSION

6.1 XMM-Newton instrument background

It can be seen from Figure 4 that the simulated data is consistent with the in-orbit data for this basic model. The MOS results are found to be more accurate at lower energies in the more advanced model as described below (see Figure 5). The difference between the single-pixel and multi-pixel events in the pn is very small due to the larger pixel size of 150 microns compared to the MOS pixel size of 40 µm. The causes of the instrument background are tabulated in Table 3, and yield some interesting results.
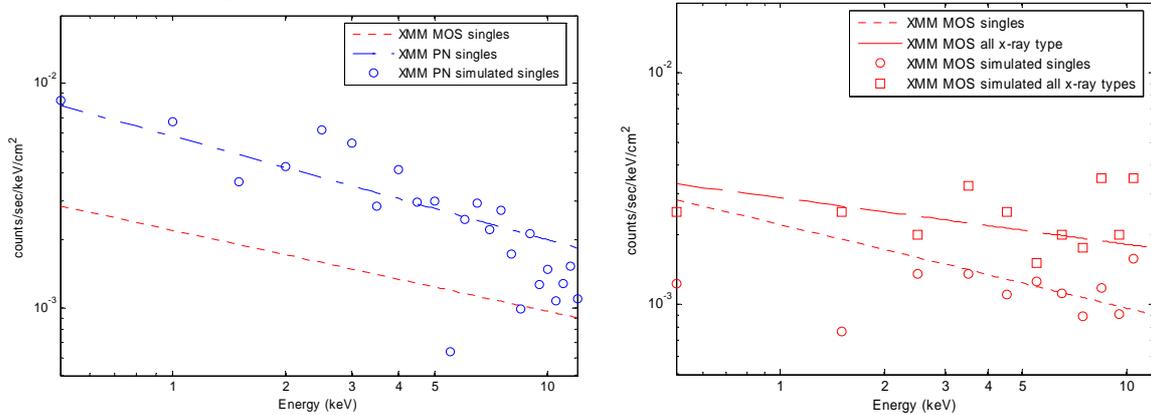

Figure 4. The initial simulated results for the XMM-Newton detectors using the basic electrodes model, with the pn results shown left and the MOS results shown right. These results were taken with incident protons at 100 MeV, 200 MeV and 400 MeV scaled as Energy^{-2} and normalised to a count rate of 2-2.5 protons per cm^2 per second (Lumb, 2002). The results show that the pn model is consistent with the in-orbit results. The MOS results for the single pixel events are slightly low below 3 keV. This is assumed to be due to the approximations in the design of the surface structure of the MOS in this early model. These results are consistent with the in-orbit data, but it is seen in Figure 5 that the more accurate model gives much better results.

It can be seen from these results that the simulation predicts that hLowEIoni (see Table 3) is the highly dominating cause of the instrument background. This implies that the factor of three difference between the count rates for the MOS and the pn is not related to the thickness of the detector, but to the effects at the surfaces of the detectors. There are several differences between the surfaces of the detectors which could cause this difference in count rate and these are investigated below.

Table 3. The main causes of the instrument background and the percentage of the single pixel events caused by these interactions. These results show the fractions of the background caused by the incident protons.

Cause of background	Geant4 ID	% in MOS	% in pn
Incident protons ionise the inner surface of the aluminium shell, ejecting electrons. These electrons are detected at the surface of the detector (range of a few microns in Si).	hLowEIoni	96.7	97
Photons produced by bremsstrahlung interactions in the aluminium shell are detected directly in the silicon.[*]	eBrem	2.5	2
Photons produced by interactions in the aluminium shell undergo Compton scattering inside the silicon and the following recoil electron is detected.[*]	compt	0.8	1.0

*The interactions leading to these points are unclear from the simulation as the particles cannot be tracked in reverse

The most obvious differences between the MOS and pn structure are in the pixel size and the front electrode/protective layer structure. In both detectors it appears that the majority of the signal is detected from the front of the detector due to the structures on the rear of the pn and the field-free region on the rear of the MOS.

The results shown below were taken with the same two models, except that the pn was altered to give a pixel width of 40 microns to match that of the MOS. From Figure 5 it is clear that the difference in pixel size is not causing the differences in background count rates between the MOS and the pn. This implies that the difference is caused by the variations in the structures on the surfaces of the two detectors.

As the differences in the background appear to be due to the surface structures of the detectors, a more accurate representation of these structures is required for the simulation. For the MOS detector, the updated layout is shown in Table 4. This new electrode structure gives an overall 40% open electrode structure. The remaining 60% is covered with the layered structure as detailed in the Table.

It would appear from Figure 5 (right-hand side) that the majority of the signal producing the instrument background in the MOS is incident through the 40% of the surface which is "open" due to the open pixel structure of the MOS CCD. In other words, 60% of the signal detected in the pn detector is not being detected in the MOS detector but is instead begin absorbed in the electrodes. As the electrodes cover 60% of the surface of the MOS it is the absorption of signal in the electrodes that is thought to be the most significant cause of the lower background.

Table 4. The more accurate model of the MOS electrodes.

Layer	MOS	Fraction of surface covered
SiO_2	0.5 µm	0.6
Si	0.5 µm	0.6
Si_3Ni_4	0.085 µm	0.6
SiO_2 layer	0.085 µm	1

A further refinement to the pn model was made, placing a 0.25mm gap between the pn detector silicon and the copper representing the printed circuit board below this. The uncovering of the rear side of the detector leads to a doubling of the background signal, which is of course to be expected with a surface dominating effect. This model does not take into account the electrode structure on the rear surface of the pn detector and thus leads to the need for further refinements.

With the same electrode structure placed on the rear of the pn the background is lowered to a more consistent level. The results suggest that the MOS can be regarded as an almost entirely front facing device (most of the signal is detected through the front surface, as from the rear side the signal is attenuated and may be subject to charge spreading) and that the pn can be regarded similarly, with a small proportion of the signal from the electrons entering through the electrodes on the rear of the detector.
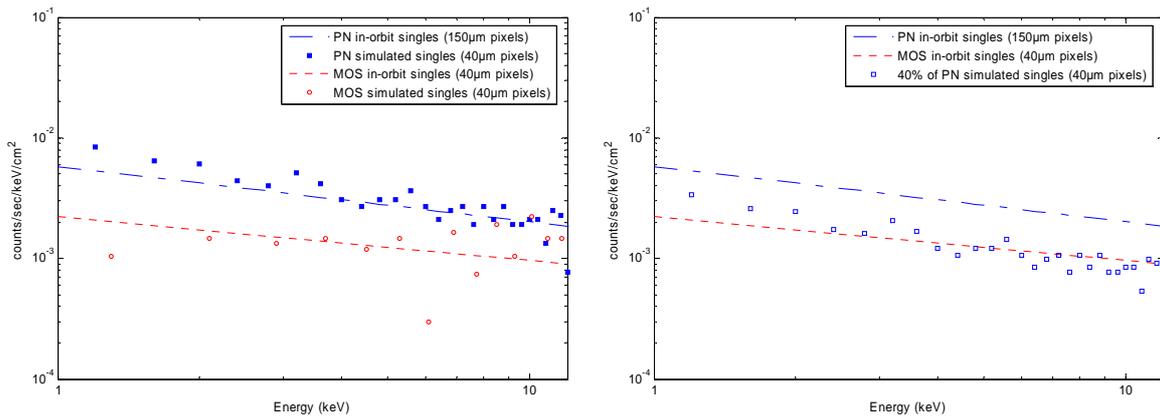

Figure 5. Simulated results (for 100 MeV incident protons only) shown against the in-orbit data. *LEFT:* The results show little variation due to the size of the pixels in the pn. The MOS results shown here are for the electrode structure shown in Table 4 and show much better consistency with the in-orbit results. *RIGHT:* 40% of the count rate for the pn is shown to compare with the MOS in-orbit data.

6.2 Suzaku instrument background

The spectra produced from the simulation (Figure 6) appear consistent with the in-orbit data and so an analysis of the main causes of the instrument background follows.
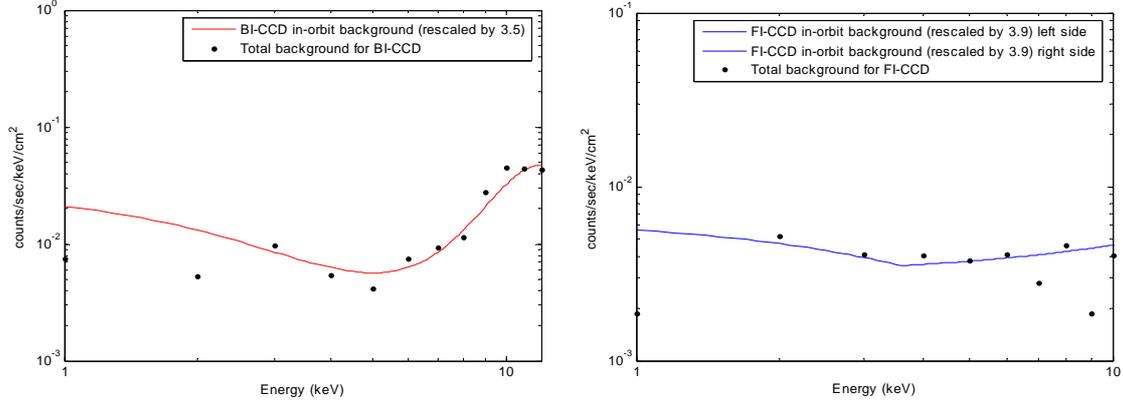

Figure 6. Simulated results for the Suzaku mission detectors. The approximations used for the surface structures of the detectors will have the greatest affect at low energies, as seen in the spectra. This is due to absorption in the surface structures having a greater impact proportional to the particle energy for lower energy particles. *LEFT:* FI-CCD results. *RIGHT:* BI-CCD results.

It was found that there are three main components to the instrument background: Compton electrons, tracks from charged particles, and electrons ionised from the aluminium shell. A description of these components is given in Table 5.

Table 5. The main components of the instrument background in the Suzaku FI-CCDs and BI-CCD. These components differ in importance between the two detectors due to the differing detector construction. It is the balance of these components which defines the spectral form.

Component	Description	Details
Compton electrons	Cosmic-ray photons pass into the silicon and the recoil electrons from the Compton interactions inside the silicon are detected as X-ray-like events.	Thicker silicon will lead to a greater number of Compton interactions. Proportional to thickness. The optimal thickness requires a balance with the Compton component, the quantum efficiency at higher energies and the peak of the component described below.
Tracks from charged particles	Minimally ionising particles passing through the silicon will leave a trail of electrons which can be detected as X-ray-like events (providing they fit the required pixel patterns). This produces a peak in the spectrum at an energy related to the silicon thickness. Front-illuminated devices will reject much of this component due to increased charge spreading in the non-depleted silicon.	Approximately 80 electron-hole pairs per micron of Si, with 3.6eV per pair: predicts peaks at 13keV (BI-CCD) and 20keV (FI-CCD), as seen in the simulated data. The peak for the XMM-Newton pn-CCD falls at 90keV (out of range of interest due to thicker detector).
Electrons ionised from the aluminium shell	Protons (and electrons to a lesser degree) passing through the aluminium shell can liberate electrons. These electrons can only travel a few microns through the aluminium so only those at the inner surface will be important. These electrons, if hitting the detector, can be detected as X-ray-like events.	These electrons will only pass through a few microns in silicon and are thus considered a surface effect. Their detection depends on the surface construction of the detector.

The components forming the instrument background in the Suzaku FI-CCDs and BI-CCD are shown in Figure 7. This figure shows qualitatively how the instrument background is formed in the CCD detectors at the Suzaku orbit and is consistent with a previous study [3]. These results are also consistent with those found here for the CCD detectors onboard XMM-Newton (see Section 6.1) which are in a higher orbit.
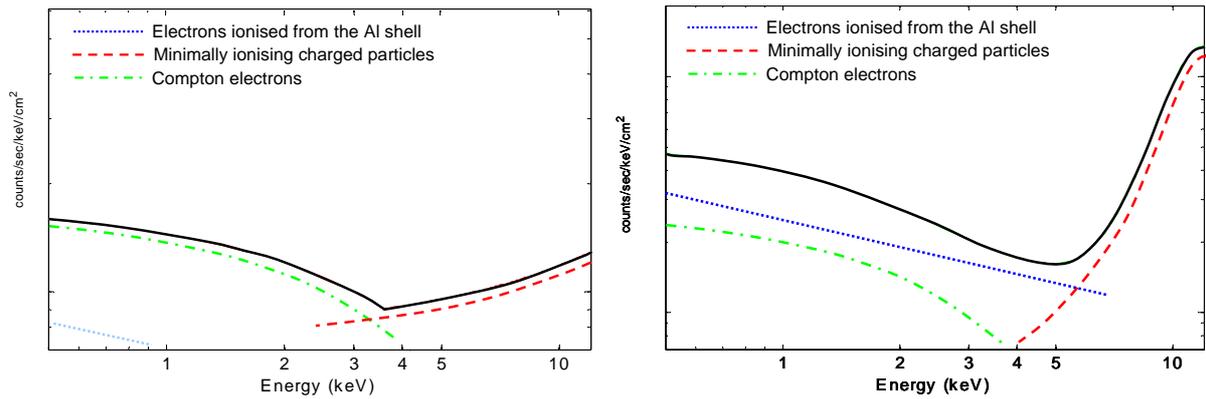
Figure 7. The processes behind the Suzaku simulated results. *LEFT:* The main constituents of the FI-CCD instrument background. The Compton electrons dominate the background at low energies. The remaining part of the background is thought to be the un-rejected charged particle background, although it is unclear as to the origin of this part of the background from the simulation without charge spreading code. *RIGHT:* The thinner silicon leads to a peak at a lower energy of approximately 13 keV seen on the right of this spectrum. All charged particles which pass through an X-ray-like pixel pattern will be detected as X-ray-like and so the peak is higher. The Compton background seen in the FI-CCD is slightly higher due to the thicker silicon, but in the BI-CCD there is also the contribution from the electrons ionised from the aluminium shell. In the FI-CCD these electrons are absorbed in the electrodes. The lack of electrodes on the front of the BI-CCD leads to these electrons being fully detected and dominating the instrument background at low energies.

Murakami *et al.* [3] discuss the generation processes which they find to be producing the instrument background in the Suzaku detectors. They do not, however, discuss the composition of the background on an energy scale basis as shown here in Figure 7, but concentrate more on a numerical summary of the overall background. Their results are consistent with those found here: in the FI-CCD Compton scattering dominates, with approximately half of the Compton recoil electrons produced by the primary cosmic-ray photons and the remaining half produced by electrons or protons interacting in the housing, and in the BI-CCD the incident electrons to the detector are mainly produced by ionisation in the housing from the cosmic-ray protons. They state that the electrons detected in the BI-CCD are blocked by the surface gate structure of the FI-CCD and as such do not make a contribution to the background. The results found here take a further step and show a more detailed picture of how this background is formed in the various regions of the energy spectrum.

7. REDUCING THE BACKGROUND IN FUTURE INSTRUMENTS

Any method which might reduce the instrument background without significant reduction of the desired signal is worth investigating in more detail. One possible method of reducing the background is the use of Z-graded shielding. This method does not affect the desired signal but may significantly reduce the instrument background.

7.1 Z-Graded shielding

A study of Z-graded shielding was published in 2004 from Elmar Pfeffermann *et al.* [6]. The following paragraph is given as a summary of this paper.

A 1 mm layer of aluminium oxide is intransparent to X-ray photons below approximately 10 keV, see Figure 8 (left-hand side). Such a layer would significantly reduce the background from fluorescence photons from outside of this layer. The fluorescence X-ray photons from the aluminium oxide layer lie below 2 keV and would therefore be detected as X-ray like signal unless otherwise absorbed. A 1 mm layer of boron carbide is intransparent to X-ray photons below approximately 4 keV, see Figure 8 (left-hand side). If placed on the aluminium oxide layer, the fluorescence X-ray photons from the aluminium oxide layer would be absorbed. The fluorescence yield of carbon and boron are of the order of 0.1 percent. The majority of the energy re-emitted from the boron carbide is in the form of Auger electrons of energy below 280 eV. These electrons can be absorbed in a layer of just several nanometres of Si or SiO_2 and would therefore be absorbed in the passivation layer of the CCD. However, any impurities in the materials can lead to an increase in fluorescence lines. Although a reduction in the strength of the fluorescence lines is clear from the above, the effect of the Z-graded shielding on the continuum is not covered in the Pfeffermann paper.

The geometry of the simulation for XMM-Newton was altered to include a 1 mm layer of Al_2O_3 inside the aluminium shell with a further 1 mm layer of B_4C inside this. The results are shown in Figure 8 (right-hand side). A significant reduction by a factor of approximately 2-3 in the background continuum is seen in the initial simulated results, although further work is required to confirm this result. Electrons ionised from the inside of the aluminium shell will be absorbed within the 1 mm layer of aluminium oxide, as from the aluminium oxide to the boron carbide, so only those electrons ionised on the inner surface of the boron carbide layer can be detected.

Although the B_4C and Al_2O_3 layers appear to reduce the level of the continuum of the background, the effect of the B_4C on the fluorescence peaks also has to be taken into consideration. B_4C and Al_2O_3 were chosen for their positive effects on the background from fluorescence, but when introducing new materials one has to be careful not to also introduce impurities to the system. Impurities in the B_4C particularly will show up in the spectrum as further fluorescence peaks and will reduce the advantage gained from any reduction in the background continuum.
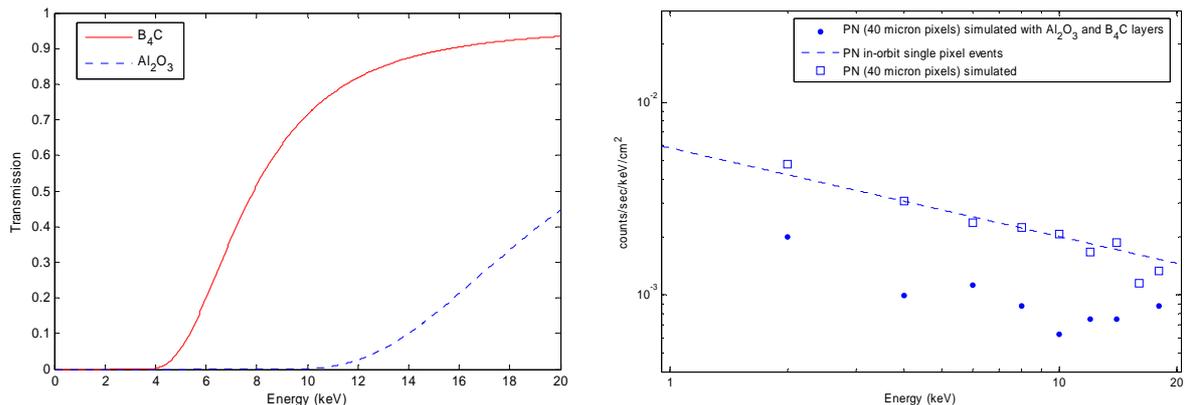

Figure 8. *LEFT:* Transmission for 1 mm layers of boron carbide and aluminium oxide. The aluminium oxide is intransparent to X-rays below approximately 10 keV and the boron carbide below approximately 4 keV. The boron carbide layer is therefore opaque to the fluorescence photons from the aluminium oxide. *RIGHT:* The inner surface of the aluminium sphere was coated with a 1 mm layer of aluminium oxide followed by a 1 mm layer of boron carbide. The simulated background for the Z-graded shielding (dots) is significantly lower than for the aluminium only shielding (squares).

For the case of the Suzaku mission, Murakami *et al.* [3] carried out tests using multi-layer shielding, consisting of beryllium and tungsten. They found a reduction in intensity of X-rays in the energy band 10-500 keV to approximately one third, but approximately double the intensity of X-rays in the energy band of 2-8 keV. They state that the total background will be reduced as long as the background is dominated by the Compton scattering. The impact of an Al_2O_3 and B_4C layer structure is not covered here for the incident particle spectrum at the Suzaku orbit.

8. CONCLUSIONS

We have analysed the instrument background from the XMM-Newton and Suzaku missions using the Geant4 toolkit. The results show that there are three main components to the instrument background (Table 5) and it is the relative dominance of these components which determines the form of the instrument background spectral continuum. The detector construction (front-illuminated vs. back-illuminated, the thickness of silicon) and the mission orbit (LEO vs. HEO) both affect the relative dominance of these components. In terms of the detector construction, for cases where the source sensitivity is important, there is a balance between the efficiency of the detection of the desired signal against the level of instrument background. The orbit determines the incident spectrum of particles and these particles will be affected by the shielding surrounding the detector.

- XMM-Newton mission (HEO):

    - Instrument background is dominated by electrons ejected from the inner surface of the shielding and spacecraft through ionisation.

    - The MOS CCDs are sensitive to electrons only from the top side, where some energy is absorbed in the electrode structures. The pn CCD is sensitive to electrons from both sides, with very little energy being

absorbed before detection on the front surface. This largely accounts for the increase in the background by a factor of 2-3.

- Suzaku mission (LEO):

    - BI-CCD instrument background is dominated at low energies (below 5 keV) by electrons ionised from the inner surface of the shielding and spacecraft (with some contribution from Compton scattered electrons), and at higher energies (above 5 keV) dominated by un-rejected minimally ionising particles passing through the detector.

    - FI-CCD instrument background is dominated at low energies (below 4 keV) by Compton scattered electrons, and at higher energies it is thought that un-rejected minimally ionising charged particles dominate.

The signal from the charged particles passing through the silicon can be reduced by either using a front illuminated CCD with a field-free region, or by increasing the thickness of the detector silicon to shift the peak away from the energy range of interest. Although the Compton induced background would be hard to reduce without using a thinner detector and hence trading on the quantum efficiency, graded-Z shielding (Section 7) may result in a reduced flux of electrons ionised from the inner surface of the shielding, as well as reducing the X-ray fluorescence, and could therefore further reduce and simplify the background. Further study is required to investigate this possibility, as there may be increased sources of fluorescence due to impurities and there is the possibility of outgassing, leading to contamination of the detector. Even with these potential problems, graded-Z shielding should be taken into consideration for future missions.

REFERENCES

1. D. H. Lumb, R. S. Warwick, M. Page, and A. De Luca, "X-ray background measurements with XMM-Newton EPIC", *A&A* **389**, 93-105 (2002)
2. M. J. Freyberg, U. G. Briel, K. Dennerl, F. Haberl, G. Hartner, E. Pfeffermann, E. Kendziorra, M. Kirsch, D. Lumb, "The EPIC pn-CCD detector aboard XMM-Newton: status of the background calibration", *SPIE* **5165**, 112-122, (2004)
3. H. Murakami, M. Kitsunezuka, M. Ozaki, T. Dotani and T. Anada, "Origins of the instrument background of the X-ray CCD camera in space studied with Monte Carlo simulation", Proceedings Vol. **6266**, *Space Telescopes and Instrumentation II: Ultraviolet to Gamma Ray*, Martin J. L.Turner; Günther Hasinger, Editors, 62662Y (2006)
4. H. Yamaguchi, H. Nakajima, K. Koyama, T. G. Tsuru, H. Matsumoto, N. Tawa, H. Tsunemi, K. Hayashida, K. Torii, M. Namiki, H. Katayama, T. Dotani, M. Ozaki, H. Murakami, and E. Miller, Proc. "The background properties of Suzaku/XIS*" SPIE Int. Soc. Opt. Eng.* **6266**, 626642 (2006)
5. T. Mizuno, T. Kamae, G. Godfrey, T. Handa, D. J. Thompson, D. Lauben, Y. Fukazawa, and M. Ozaki, "Cosmic-Ray Background Flux Model Based on a Gamma-Ray Large Area Space Telescope Balloon Flight Engineering Model", *Astrophysical Journal* **614**, 1113–1123, (2004).
6. E. Pfeffermann, P. Friedrich, M. Freyberg, G. Kettenring, L. Krämer, N. Meidinger, P. Predehl and L. Strüder, "Shielding of cosmic ray induced background in CCD detectors for X-ray astronomy", Proceedings Vol. **5501**, *High-Energy Detectors in Astronomy* (2004)